Applied Geomatics
https://doi.org/10.1007/s12518-024-00561-y

ORIGINAL PAPER

# Using structure from motion for analyzing change detection and flood events in the context of flood preparedness: a case study for the Laufer Muehle area at the Aisch river in Germany for conducting near real-time analyses

**Michael Kögel**[1] · **Dirk Carstensen**[1]

Received: 27 June 2023 / Accepted: 3 March 2024


**Abstract**
Recent flood events (FE) in Germany have shown that the extent and impact of extreme flood events cannot be estimated solely based on numerical models. For analyzing the development of such an event and to develop and implement safety measures more efficiently, additional data must be collected during the event. Within the scope of this research, the possibilities of near real-time recording using an unmanned aerial vehicle (UAV) and data processing with the Structure from Motion (SfM) method were tested in a case study. Different recording parameter combinations were tested in the Laufer Muehle area on the Aisch river in Germany. The focus of the investigations was the identification of a parameter combination that allows a short recording interval for aerial imagery. Based on these findings, the identification of changes in the study area by comparing multitemporal photography (flood prevention), as well as the recording of flooded areas during a FE should be possible. The accuracy analysis of the different parameter combinations between two point clouds as well as the process of change detection was done by a Multiscale Model to Model Cloud Comparison (M3C2) and including ground control points. As a result, a parameter combination was identified which led to the desired results in the study area. The processes were transformed into fully automated and scripted workflows. The results serve as a basis for establishing a workflow for near real-time analyses in future studies.

**Keywords** Structure from motion · Flood event · Change detection · M3C2 · Real-time

## Introduction

In the context of planning flood protection systems, watercourse maintenance, or in situ analysis and investigation of the effects of flood events (FE), it is imperative to have an extensive and detailed basis of data on a large spatial and temporal scale. Reliable data of terrain information (terrestrial and bathymetric), stream gauging station observation sites, vegetation, and built-up areas are necessary to best analyze area-related conditions or to implement these conditions in planning and modeling.

According to the current state of affairs, these surveys are usually carried out based on available surveying databases, which only reflect the condition of the object or area to be surveyed at the time of the survey. For the most part, these surveys record the terrain heights and the building dimensions at a few points that are significant and relevant for the investigations and in a predefined measurement grid. Important information, such as the vegetation, structural condition/damage, and deformations of the foreland of flowing waters as a result of mass transport (erosion, sediment accumulation), is lost in the process. Such information is, however, prerequisite for an adequate implementation of the current condition in flood investigations and for ensuring meaningful results. Usually, it is not possible to collect this data and information quantitatively within the framework of periodical (twice a year) watercourse monitoring.

✉ Michael Kögel
michael.koegel@th-nuernberg.de

Dirk Carstensen
dirk.carstensen@th-nuernberg.de

[1] Technische Hochschule Nürnberg Georg Simon Ohm Institute of Hydraulic Engineering and Water Resources Management, Nuremberg, Germany

Published online: 13 March 2024

The flood events at the rivers Aisch and Zenn, the Franconian Rezat, in North Rhine-Westphalia (NRW) and Rhineland-Palatinate (RP), in Bavaria, Thuringia or Saxony in July 2021 have, besides the extreme meteorological and hydrological impact from climate change, illustrated the importance and primary influence of the mentioned factors on the course of FE.

During the FE in Middle Franconia in the period between July 9, 2021 and July 13, 2021, the rivers Aisch, Zenn, and Franconian Rezat overflowed their banks significantly and flooded large parts of the river basins.

The event, which according to current information resembled a hundred-year flood ($HQ_{100}$), was the cause of extensive flooding in the area of the Aisch river (approx. 30–35 km west of Nuremberg). At the gauging station Markt Bibart, the highest amount of precipitation in the study area was recorded during the event with 88.61 l/m². In the two weeks before, a total of only 47.56 l/m² was measured. Thus, almost twice the amount of precipitation was recorded during the flood event than in total in the two preceding weeks. Despite the widespread flooding, only limited (property) damage was recorded. No information and data were available on the morphological processes (accumulation, erosion) at the time of the investigations, since the technology proposed here could not yet be applied.

Other parts of Germany were affected even more severely by a flood event. After a heavy rain event in the Ahr valley (North Rhine-Westphalia, Rhineland-Palatinate) in the period between July 14 and July 15, 2021, a flash flood occurred and caused enormous damage to property and people.

In the above cases, it is not yet possible to fully clarify all the circumstances, causes, and effects of the events. However, it is likely that the extreme precipitation may not have been fully covered by existing numerical models. Also, there could be an incomplete database (topography and vegetation) and outdated inventory records in the models. Due to changing weather patterns as a result of climate change, the volatility of such events has increased significantly and statistically calculated infrequent FE are occurring more frequently and more pronouncedly.

To be able to implement this information in the long term and sustainably, recurring recordings and investigations are necessary, for example in monitoring using permanent observation points with highly accurate and state-of-the-art surveying methods. In the context of digitalization, new and optimized measurement methods and models are therefore required to record and map relevant information promptly and to transfer it into measures.

Photogrammetric reconstruction with the Structure from Motion method (SfM) is a technique that can be used to map surfaces and objects. Using mathematical operations, it is possible to create a three-dimensional object (for example point cloud (PC), digital surface model (DSM), or digital terrain model (DTM) based on spatially overlapping photos. This method was first introduced in the 19th century (Meydenbauer 1867). At that time, it was very costly to determine geometric properties based on photos. Now, computers can process a large amount of data in a short time by using appropriate software solutions. Together with tacheometry and 3D laser scanning, these three techniques are mainly used to generate 3D datasets (Triantafyllou et al. 2019).

3D laser scanning is another method to record extensive terrain information in three dimensions. With this methodology, the terrain is recorded by an optical light beam. The light beam emitted by the device is reflected by an object and sent back to the measuring device. By comparing the emitted and the received light beam, conclusions can be drawn about the distance of the measuring device to the object, with the distance determination considering the speed of light. For example, a common method for laser-based distance determination is the time-of-flight method or light detection and ranging (LIDAR, Vosselman and Maas 2011).

LIDAR acquisition can be terrestrial (terrestrial laser scanning, TLS) or airborne (airborne laser scanning, ALS). Since photogrammetry and laser scanning are complementary measurement techniques and have applications in many research disciplines, extensive research has already taken place to compare and combine the corresponding datasets (Baltsavias 1999a; Cawood et al. 2017; El-Din Fawzy 2019; Grussenmeyer et al. 2008; Luhmann 2013; Talha and Fritsch 2019; Waele et al. 2018).

Photogrammetric reconstruction of objects offers the advantage of extremely realistic visual mapping and the results can be combined and complemented in many ways with other datasets, for example from terrestrial (TLS) or airborne (ALS) laser scanning. Complementary data analysis as well as extensive comparisons of measurement techniques have already been performed in diverse disciplines such as surveying (Mulsow et al. 2019), archaeology (Marín-Buzón et al. 2021), cave surveying (Kögel et al. 2022), and civil engineering (El-Din Fawzy 2019).

Today, extensive and photorealistic survey datasets can be generated using measurement techniques such as 3D laser scanning and photogrammetric reconstruction using the SfM method. The resulting data is promising for the analysis of changes in a study area (change detection, CD).

According to Dinkel et al. (2020), the CD process can be divided into three main steps:

1. co-registration
2. noise detection
3. detection of significant changes.

In co-registration, two data sets (for example two PC) are aligned with each other. A common method is the application of an iterative closest point algorithm (Fischler and Bolles 1981), in which a point cloud is iteratively aligned to a reference dataset. In Rusinkiewicz and Levoy (2001) different methods and variants of such algorithms are explained.

While co-registration can significantly improve results from the SfM process (Nota et al. 2022), it can degrade CD results in some circumstances (Lague et al. 2013). Because the purpose of these studies was to investigate the potential for detecting CD using different flight parameter constellations, independent of optimizations using external data sets, the potential for optimization using co-registration processes was not investigated at this time.

Detection of differences in multitemporal imagery can be performed in two (photographic imagery) or three dimensions (geometric datasets, PC, DTM, etc.). The basic differences between the two methods according to Qin et al. (2016) are explained in Table 1.

In a 2D data comparison, statements about the height vector and thus the volumetric information of change detection are only possible to a limited extent. In addition, terrain changes below cover, for example in the form of vegetation cover by tree canopies, cannot be detected by two-dimensional nadir images. Since these changes also need to be detected, as well as for the previous reason, 3D analysis was chosen for these investigations.

**Table 1** Overview of differences between 2D and 3D CD (Qin et al. 2016)

| | 2D CD | 3D CD |
|---|---|---|
| Data sources | • 2D panchromatic/ spectral images, 2D vector data | • 3D point clouds, digital surface models, stereo images, multi-view images, 3D models, etc. |
| Application scale | • Generally applied to LTMR images at a landscape level<br>• Limited applications in very high resolution at individual building level | • Generally applicable to data with any resolution<br>• Applicable for data from oblique views |
| Advantages | • Well-investigated<br>• Easy to collect data<br>• Easy to implement | • Height component robust to illumination differences<br>• Free of perspective effect even for VHR data<br>• Provide volumetric differences |
| Disadvantages | • Strongly affected by illumination and atmospheric conditions<br>• Limited by viewing angles, perspective distortions | • Unreliable 3D information may result in artifacts<br>• Partly still expensive data sources |

The occurrence of noise in PC data sets, as the presence of scatter points, can lead to a misinterpretation of the results in the context of CD. Since the points resulting from noise will most likely not be present in the data sets of a time-shifted recording, this is considered a change in the study area, although this leads to a misinterpretation. Especially vegetation and other easily movable objects increase the generation of noise because their movement can cause minimal changes even during a running recording, which are interpreted by the system as actual measurements.

Within the scope of this research, the possibilities of aerial photogrammetry-based long-term surveying of areas at risk from flooding were investigated. The terrain of a defined study area at the Aisch river ( see Sect. Laufer Muehle ) was photogrammetrically surveyed at different times. The surveys were carried out using different combinations of flight parameters. In this way, optimized parameters were determined, by which the terrain can be recorded with low time expenditure (both in the context of the data acquisition and in the post-processing) and adequate accuracy. The parameters were determined by comparison with a high-resolution reference dataset.

The basic aim was to ensure the shortest possible processing time for both data acquisition and data processing (post-processing). This should make it possible to make relevant decisions during a flood event in the shortest possible time intervals and to be able to initiate appropriate measures under certain circumstances.

Differences (erosion and accumulation, repositioning of objects, vegetation changes) were detected and categorized by intersecting the multitemporal images. The focus of the investigations was to automate the various processes as far as possible so that an analysis can be carried out highly frequently and in near real-time in the event of flooding.

## Study area

### Aisch river

The Aisch river is classified as a 1st order water body (Bayerische Staatskanzlei 2010) and originates about 1.25 km south-southeast of Schwebheim (Bayerisches Landesamt für Umwelt 2022a). It has a length of approx. 84.29 km and flows into the Regnitz about 2.1 km south-southeast of Buttenheim. The river basin of the Aisch river covers 1,006.31 km² (Bayerisches Landesamt für Umwelt 2016) and is characterized by a rural pond landscape (Bayerisches Landesamt für Umwelt 2011).

## Laufer Muehle

Due to the size of the Aisch river basin, it was not possible to include the entire area in these investigations. The focus was therefore on surveying a small area (Laufer Muehle), which could be captured by an aerial drone (in this case a quadrocopter) with a time-cost effective manner. The scalability of the investigation results to a larger investigation area is discussed in Sect. Future prospects. The actual possibilities in this context need to be determined in further investigations.

Starting from the origin of the Aisch river the Laufer Muehle is located at 70.6 riv. km. The area is a small village through which the Aisch river runs directly. A weir is located at the western end of the village and a stream gauging station of the Kronach Water Management Office (Bayerisches Landesamt für Umwelt 2022b) is located approx. 90 m from the weir. The location of the study area is illustrated in Fig. 1.

The area was particularly well suited for the investigations, mainly because it is very much characterized anthropogenic influences. This made the expectation reasonable that changes in the terrain would be detectable between the multitemporal surveys carried out and that these changes would be identifiable in the different recordings. In addition, this area is regularly affected by flood events, making it likely that the recording methodology described here could be applicable in the event of local flooding.

The water levels of the Aisch river at Laufer Muehle are recorded at the stream gauging station in 15-minute time intervals, which provides good plausibility of survey results. Table 2 lists the main values of water level and discharge at the Laufer Muehle stream gauging station.

The reporting levels at the Laufer Muehle stream gauging station are given as follows according to Bayerisches Landesamt für Umwelt (2023):

**Notification level 1: 400 cm**

Small localised outburst floods.

**Notification level 2: 430 cm**

Agricultural and forestry areas flooded or slight traffic obstructions on main roads and municipal roads.

**Notification level 3: 480 cm**

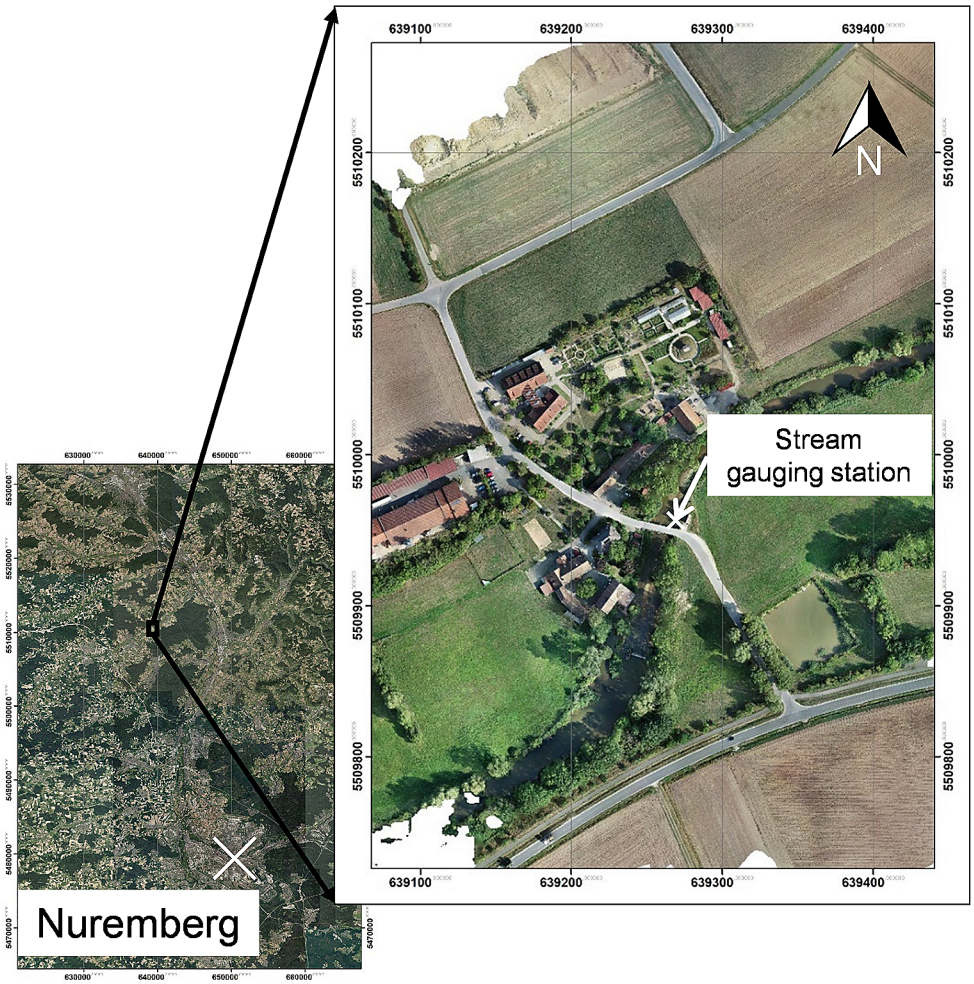


**Fig. 1** Location of the Laufer Muehle area and the stream gauging station. (source: orthophoto left image: www.geoservices.bayern.de, raster information according to reference system EPSG 25,832; orthophoto right image: results from own airborne images)

**Table 2** Main values of water level and discharge

| | Main values (1964–2012) Water level [cm] | | | | Main values (1927–2012) discharge [m³/s] | | |
|---|---|---|---|---|---|---|---|
| | winter | summer | year | | winter | summer | year |
| **LW** | 170 | 169 | 169 | **NQ** | 0,61 | 0,30 | 0,30 |
| **MLW** | 221 | 211 | 209 | **MLQ** | 2,06 | 1,55 | 1,47 |
| **MW** | 278 | 237 | 258 | **MQ** | 7,00 | 3,28 | 5,13 |
| **MHW** | 453 | 383 | 464 | **MHQ** | 63,30 | 28,30 | 70,80 |
| **HW** | 563 | 548 | 563 | **HQ** | 218,00 | 360,00 | 360,00 |

LW = low water; MLW = mean low water; MW = mean water; MHW = mean high water; HW = high water; NQ = low water discharge; MLQ = mean low water discharge; MQ = mean water discharge; MHQ = mean high water discharge; HQ = high water discharge; at the Laufer Muehle stream gauging station (Bayerisches Landesamt für Umwelt 2022b)

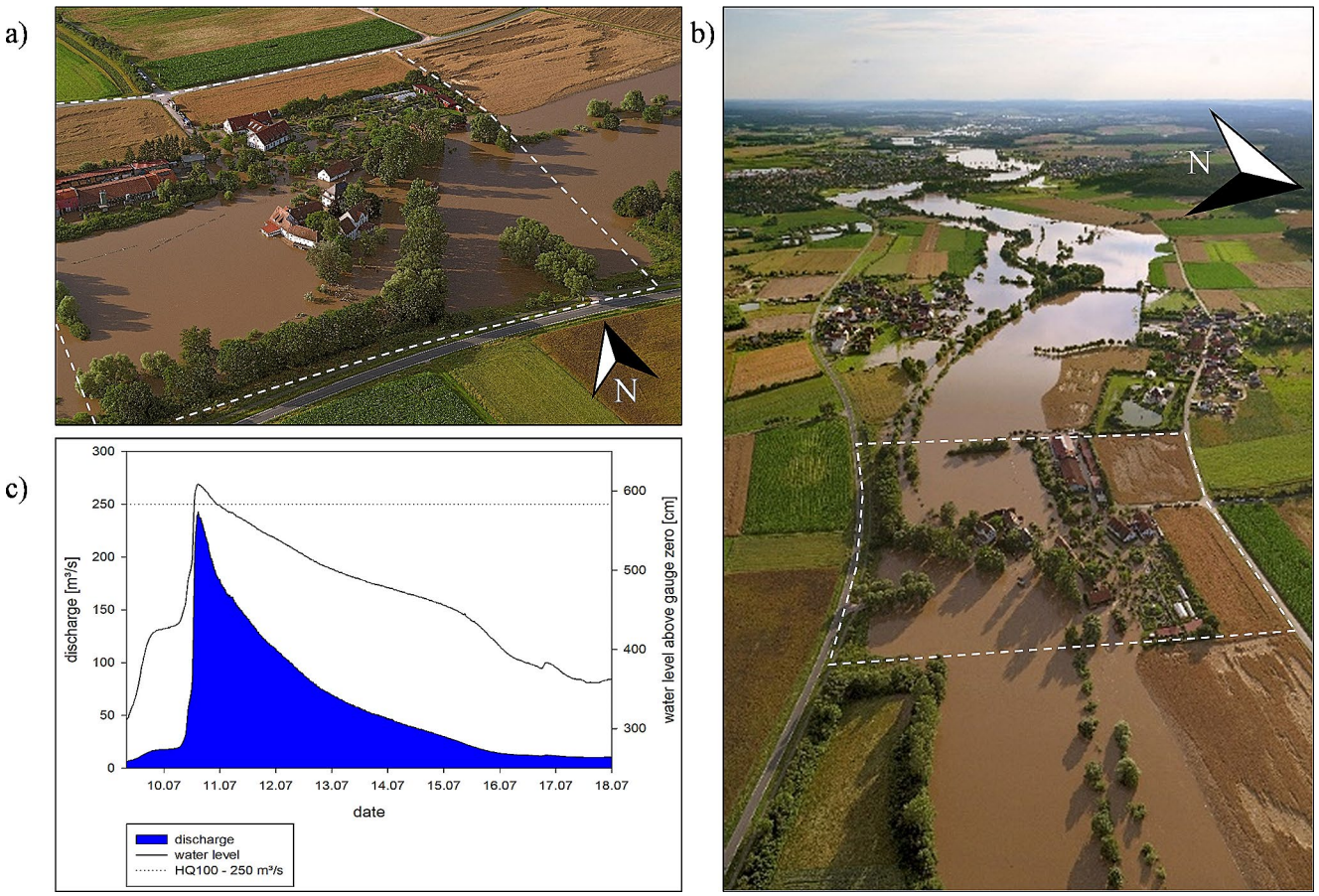


**Fig. 2** **a** and **b** Flooding of the Aisch river on July 12, 2021, in the area of Laufer Muehle with the area of investigation indicated. (source of photos: Wasserwirtschaftsamt Nürnberg 2021). **c** Discharge and water level at the stream gauging station Laufer Muehle during the flood event in July 2021 with the respective 100-year flood ($HQ_{100}$) discharge indicated (Bayerisches Landesamt für Umwelt 2022b)

Individual built-up areas or cellars flooded or closure of inter-urban traffic routes or isolated use of water or dam weirs required.

**Notification level 4: 540 cm**

Built-up areas flooded on a large scale or large-scale deployment of water or dam weirs required.

## Flood event 2021

As already mentioned in Sect. Introduction, large-scale flooding in the area of the Aisch resulted from the FE in July 2021. Accordingly, the area of Laufer Muehle was also flooded over a large area. Figure 2 shows aerial photographs from this FE and visualizes corresponding discharge and water level parameters.

It is important to note that the stream gauging station starts to become circumferential at a discharge of about 28 m³/s. According to Bayerisches Landesamt für Umwelt (2022b) the validity of the gauge values for $Q > 28$ m³/s can therefore not be evaluated with absolute certainty, as the water level at the station remains approximately the same, while the discharge keeps increasing.

## Methods

### Measuring device

#### Data acquisition with unmanned aerial vehicle

An unmanned aerial vehicle (UAV) of the type DJI Phantom 4 RTK was used for data acquisition. The device is equipped with a camera with a 1" CMOS sensor and a resolution of 20 MP and can be operated both manually and autonomously. The autonomous control makes it possible to give the device predefined trajectories, which are subsequently flown independently by the device. Due to the spatial definition of these trajectories, data recordings can be performed again at a later time at approximately the same positions, which makes the potential for comparison and superposition of these multitemporal recordings very high.

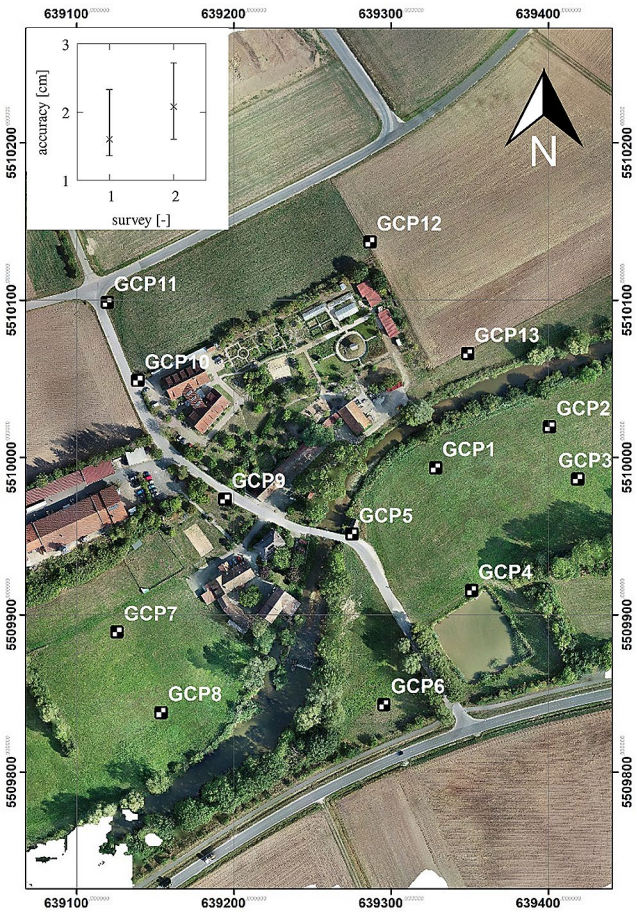


**Fig. 3** Location and accuracy (3D; mean, max and min value) of the georeferenced GCP at surveys 1 and 2 in the study area

Based on the acquired photo data, three-dimensional terrain data was derived by using the SfM post-processing method with Agisoft Metashape Professional 1.8.4. The date of the surveys was selected in such a way that the study area was recorded in consideration of high (summer, survey 1) and low (autumn, survey 2) vegetation. In this way, seasonal fluctuations could also be taken into account and represented when detecting changes.

#### Using ground control points for plausibility check of measurement data

In the course of this research, 13 GCP (flat plates with a coded marking) were placed in the survey area during each survey. They were georeferenced using global navigation satellite systems (GNSS) and real-time kinematic (RTK) with the real-time positioning service (high-precision real-time positioning service, HEPS) of the German Satellite Positioning Service (SAPOS). This type of position determination is used in diverse measurement devices in both terrestrial (Mancini and Salvini 2020), bathymetric (Xie et al. 2021), and hybrid data acquisition (Kutschera et al. 2018).

The GCP were implemented in the bundle adjustment to generate an optimized reference dataset (dataset M1), which would provide the most accurate results when analyzing changes in the study area and therefore be used as a comparison dataset (Sect. M3C2: parameter selection for distance comparison between mission data and georeferenced GCP) to validate the SfM results of other missions. In case of the missions were the GCP were not implemented in the bundle adjustment, the GCP were used as check points to validate the accuracy of the data sets.

The GCP were surveyed using a GNSS rover with RTK connectivity. Except for GCP11, which was intentionally offset by approximately 1 m from the previous survey for accessibility reasons, the GCP in survey 2 were placed at nearly the same position (distance < 0.10 m) as in survey 1. Figure 3 shows the location and the accuracy of the GCP in the survey area.

The use of GCP usually requires a significant amount of time and is often the largest time commitment associated with photogrammetric acquisition in a study area (Forlani et al. 2018). Also, proper positioning of GCP, especially in the context of terrain survey during a flood event, can be difficult, or only possible at high safety risk. Aware that higher accuracy of the computational results could have been achieved by integrating the GCP into the SfM process, the GCP were therefore primarily used to evaluate the accuracy

of the generated PC as well as to generate the optimized reference dataset M1.

An initial assessment of the accuracy of the reconstructed datasets was made by comparing them with the GCP surveyed in the field (Sects. M3C2: parameter selection for distance comparison between mission data and georeferenced GCP and M3C2: accuracy analysis by distance determination between M5, M16-M17 with GCP and reference dataset M1).

## Selecting flight and data acquisition parameters

In the context of the concept described here for long-term observation using aerial photogrammetry, the area of the Laufer Muehle was recorded with different parameters. The selection of the parameters was dependent on the desired outcomes:

1. analysis of changes in the study area, both morphological and anthropogenically influenced.

2. high-frequency recording during a flood event for the analysis of the development of the flood progression.

As mentioned in Sect. Introduction the basic aim was to ensure the shortest possible processing time for both data acquisition and data processing (post-processing). This approach facilitates timely decision-making during a flood event, minimizing the time intervals for relevant actions to be taken. The parameters had to be chosen in a way that the desired results can be achieved quickly, facilitating the initiation of appropriate measures when necessary. This should make it possible to make relevant decisions during a flood event in the shortest possible time intervals and to be able to initiate appropriate measures under certain circumstances. Thus, the parameters had to be chosen in a way that the results can be achieved with as little time as possible.

Concerning the identification of multitemporal changes, the geometric aspects of the study area had to be sufficiently represented in all three dimensions. This applied to the results of survey 1 as well as to the comparison states of survey 2.

Recording the vertical component of water is fundamentally difficult for various reasons. Especially under uncontrolled conditions, light refraction effects as well as the constant movement of the water ensure that the photogrammetric evaluation of the image data leads to inaccurate, wrong, or even no results at all. In the context of floodplain assessment, however, the positional components of water can be well derived from orthographic images. When the spatial position of the water surface is known, it can be intersected with terrain information. For example, the location of the bank line in the terrain can be determined using orthophotos. The corresponding terrain elevation of the bank line can be derived from a digital elevation model. By interpolating this terrain elevation onto the water surface, a height can be assigned to it. This information can then be used to determine water depths.

The relevant flight parameters for the photogrammetric surveys used in this research are listed below:

- flight mode (normal grid (NG) / double grid (DG)).
- flight altitude.
- ground sampling distance (GSD).
- flight velocity.
- camera tilt.
- horizontal overlap.
- vertical overlap.
- shutter priority.

The selected flight altitude is decisive for the level of detail with which a survey area is imaged. The resolution (ground sampling distance, GSD, Eltner et al. 2022) with which the surface is imaged results depending on the inner orientation of the camera and the flight altitude.

Concerning the mentioned parameters, different flights (missions) were carried out, considering varying flight parameters. This enabled the determination of the minimum necessary parameters to carry out the planned analyses while maintaining high accuracy. A total of 17 different parameter constellations were investigated, while only the relevant examples (M1, M5, M16 and M17) will be further discussed.

Based on findings from past investigations, the parameters for M1 were chosen (low flight altitude and DG-flight mode) in such a way that the data set with the highest accuracy would most likely result from this flight. To further optimize the results of M1the processing of the data was performed considering GCP within the SfM process (manually setting the coordinates for each GCP). The data of M1was used for the accuracy analysis of the other missions. This made it possible to determine the effect and intensity of the different flight parameters on the accuracy of the reconstructed geometries.

The most relevant results regarding accuracy when compared to the reference dataset M1, as well as the flight duration and the resulting number of images, originated from the parameter combinations of M5, M16, and M17. While the parameter combination of M1 particularly aimed for high accuracy, it cannot be used during a flood event due to the long flight duration and the resulting high number of images and processing time.

M5 was conducted at a flight altitude of 80 m in NG flight mode. It remained within a time-economic acceptable range concerning the flight duration and the number of images. Missions M16 and M17 were selected due to their ability to efficiently cover the area at a flight altitude of 110 m, achieving comprehensive coverage with a relatively low number of images. The two missions differed only in terms

of the different flight modes (NG and DG) and the resulting number of images.

Table 3 shows the flight parameters of the mentioned missions as well as the required flight duration (specified by the flight software) and the resulting number of images.

## Data processing

For the photogrammetric computation of three-dimensional PC using the SfM method the application Agisoft Metashape (Agisoft 2022a) was used, because extensive experience in its use was available, especially from previous research. In addition, the software offers different interfaces, for example with the Python programming language (Agisoft 2022b), which allows automated processing procedures by script execution. In terms of long-term observation, this offers great potential, as optimized comparison and analysis processes can be applied quickly and in a targeted manner.

The basic principle of photogrammetry is already extensively described in the literature, for example, in Eltner et al. (2022), Wiggenhagen and Steensen (2021) and Luhmann (2018).

Survey areas usually differ in their characteristics from each other and the acquisition conditions (for example, resulting from weather conditions) can lead to different calculation results despite the same acquisition and processing parameters during PC generation. Thus, measuring the quality of terrain models is a complex task due to the large number of variables involved (Forlani et al. 2018) and the additional dependence of the quality of the results on the conditions of the different study areas. Accordingly, a generally valid statement considering all relevant aspects cannot be given by a single study (Forlani et al. 2018).

Consequently, the appropriate study parameters must always be adapted based on the study area. An approach to analyzing the accuracy of computational results from aerial surveys with different survey parameters is given in Mora-Felix et al. (2020). Accuracy studies on the quality of the DJI Phantom 4 RTK GNSS system were performed in Przybilla and Bäumker (2020).

### Determination of the SfM parameters and the processing sequence

As already explained in Sect. Selecting flight and data acquisition parameters, a variety of factors during data acquisition influence the photogrammetric work scope, the data accuracy as well as the duration of this process. Likewise, the computational parameters in the SfM process in conjunction with the mentioned factors affect the reconstructed 3D PC. Due to a large number of factors, it was decided in these investigations to use parameters that have led to good results in past investigations. It cannot be excluded that optimization of these parameters can lead to an improvement of the results, or that a reduction of the accuracies of the individual parameters leads to an insignificant change in the imaging accuracy of the calculation results, which, however, can lead to significantly shorter processing times and thus possibly to an even better implementation of the investigations. This aspect will be discussed again in Sect. Future prospects

Based on findings from past studies, the downscale parameter was set to 2 (Medium) when aligning the photos (matchPhotos) and to 2 (High) when generating the depth images (buildDepthMaps) (Agisoft 2022a). This factor describes the scaling of the photos in the SfM process and specifies whether an image is used in full resolution (downscale = 0) or reduced form (downscale ≥ 1).

A high degree of accuracy results in principle in a higher accuracy of the calculation results, but also in a significant increase of the time needed for data processing as well as in a higher number of points of the resulting PC (Agisoft 2022a).

The generated and exported dense PC for each of the performed missions were used for the localization and identification of changes (CD) in the study area.

During the SfM process, a confidence value was calculated for each point of the PC, which, based on the selected settings, reflects the number of the depth maps involved in the point generation process and show how reliably a point represents reality. The confidence values can range between 1 and 255, with 1 indicating very low confidence and vice versa. It was assumed that at least filtering the points with the lowest mapping accuracy (confidence value = 1) would

**Table 3** Flight parameters of the missions M1, M5, M16-M17 with M1 optimized with GCP

| Mission | Flight mode | Flight altitude [m] | GSD [cm/Pixel] | Flight velocity [m/s] | Camera tilt [°] | Horizontal overlap [%] | Vertical overlap [%] | Shutter priority [s] | Flight duration [min] | Number of images [-] |
|---|---|---|---|---|---|---|---|---|---|---|
| **M1** | DG | 50 | 1.37 | 3 | 60 | 60 | 80 | no | 51:45 | 950 |
| **M5** | NG | 80 | 2.19 | 4 | 60 | 60 | 80 | no | 14:00 | 214 |
| **M16** | NG | 110 | 3.01 | 4 | 60 | 60 | 60 | no | 10:04 | 59 |
| **M17** | DG | 110 | 3.01 | 4 | 60 | 60 | 60 | no | 15:24 | 90 |

lead to a significant improvement in the reconstruction results. The following analyses were therefore conducted on the unfiltered and the filtered point cloud.

### Three-dimensional comparison of multitemporal terrain data sets - M3C2

The presence of vegetation and seasonal effects for CD analysis, both between data sets from data acquisitions close in time and far apart in time, significantly complicates the proper categorization of distance determination. Influenced by weather, short-term movements of vegetation (leaves, branches) can occur even during a single data acquisition process, leading to errors in the SfM process. In the long term, additional seasonal effects (vegetation growth and shrinkage, snow accumulation) can occur (Qin et al. 2016). Such change is usually not part of the desired change analysis, but can sometimes lead to significant distance differences between multitemporal datasets.

In the course of these investigations, the aim was to determine differences or discrepancies between multitemporal photos. Since important comparative data would be neutralized in the course of data filtering, the investigation was conducted with the aim of comparing largely unfiltered data sets and the data filtering was primarily related to scattering points (noise). Especially in connection with the presence of vegetation, however, this resulted in difficulties in distinguishing between constructive or terrain-specific changes and vegetation changes caused by seasonal effects (see Sect. Change detection in the Laufer Muehle area).

Since the localization of the measurement points at the same location is impossible with multitemporal measurement data recordings, it is necessary to model the terrain locally for the distance comparison. The problem of distance comparison based on measurement points with different localities is discussed in Lague et al. (2013).

A goal-oriented application for distance determination between two PC datasets is provided by the comparison through the Multiscale Model to Model Cloud Comparison (M3C2) method. It is described in Lague et al. (2013) and Winiwarter et al. (2021), among others, and is characterized in particular by the fact that it.

- determines the distance directly through the PC, without meshing or gridding,
- determines the local distance between two PC along the normal surface direction, which tracks the 3D variations in surface orientation,
- generates a confidence interval for each distance measurement depending on the roughness of the PC and the registration error.

In this method, the orientation of a single point (normal) is calculated based on adjacent points within a region of diameter D (normal scale). Parallel to the normal, a cylinder with height h (max depth) and diameter d (projection scale) is generated with the center at the selected point. Within this cylinder, points are defined in the PC to be compared and averaged for the difference determination (Lague et al. 2013).

Extensive research on the accuracies and procedures of different distance determination methods in the context of CD is described in Qin et al. (2016) and James et al. (2017) among others.

### M3C2: sensitivity analysis to determine appropriate parameters for distance computation between

The investigation aimed to determine parameters that reflect the difference between two PC to be compared with the smallest possible error. For this purpose, a total of 20 variations (cases) with different M3C2 parameter combinations were examined to find a combination with low RMS value. This sensitivity analysis resulted in the parameter combination case 21, which was used for the subsequent distance comparisons. The parameters of case 21 are presented in Sect. M3C2: sensitivity analysis of the parameters used to calculate differences between M5, M16-M17 and the reference data set M

### M3C2: parameter selection for distance comparison between mission data and georeferenced GCP

A first assessment of the accuracy of the calculation results could be achieved by comparing them with the GCP placed in the field. The distance determination was carried out based on the vertical distance of the GCP to the respective comparison point cloud of the individual missions (max depth = 1.0 m; projection scale (d) = 1.0 m; no normal computation due to vertical distance computation). The results are presented in Fig. 5.

### M3C2: accuracy analysis of mission data by comparison with data set M1

To determine the accuracy of the SfM calculation results, M3C2 distance computation was performed in each case using the parameters determined and optimized in the sensitivity analysis (Sect. M3C2: sensitivity analysis of the parameters used to calculate differences between M5, M16-M17 and the reference data set M1), for both the unfiltered and the filtered data sets. The comparison was performed by determining a normal distribution function based on the determined distances of each measurement point. In this

way, the distribution of the calculated distances could be displayed and the mean value of the deviations between the data sets could be determined. In addition, the standard deviation and the root mean square (RMS) were determined.

#### Data filtering using low change detection result values

There are different approaches for identifying and filtering noise data, which, among other things, take into account the inaccuracies that occur during the analysis processes and explicitly use them as limiting parameters for the analysis. As the goal of these analyses was to identify significant changes (assumption: significant change when $-0.25\ \text{m} \leq d \leq 0.25\ \text{m}$ with d being the distance between two multitemporal data sets), measurement points with M3C2 differences within the interval were removed from the data sets.

### Processing sequence for the identification of CD in the area of Laufer Muehle

Figure. 4 illustrates the workflow (data acquisition and processing) described in the previous sections

## Results

### 3D reconstruction with SfM

As a result of the 3D reconstruction, an unfiltered and a filtered (using confidence value as a filtering parameter, see Sect. Determination of the SfM parameters and the processing sequence) dense PC were available for each of the conducted missions. Table 4 shows the point counts (unfiltered and filtered), the percentage of filtered points to total unfiltered point counts, and the point difference between surveys 1 and 2 for each of the respective missions.

### M3C2: sensitivity analysis of the parameters used to calculate differences between M5, M16-M17 and the reference data set M1

Table 5 shows the final parameters from the sensitivity analysis (case 21) as well as the corresponding calculation results when comparing the distance between the reference PC from survey M1 and the PC from survey M16.

### M3C2: accuracy analysis by distance determination between M5, M16-M17 with GCP and reference dataset M1

Figure 5 shows the results from the unfiltered and filtered (conf) M3C2 distance determinations between M5, M16-M17 and M1 using the optimized parameters shown in Table 5. In addition, the results of the M3C2 distance comparison using the GCP as check points and the parameters mentioned in Sect. M3C2: parameter selection for distance comparison between mission data and georeferenced GCP are presented.

### Change detection in the Laufer Muehle area

Figure 6 illustrates the areas of significant change as a result of the CD for the data sets M1 (highest accuracy due to implementation of GCP) and M17 (the most effective parameter constellation in terms of recording time and accuracy, see Sect. Determination of suitable recording parameters for photogrammetric surveying in the Laufer Muehle area).

Figure 7 and Fig. 8 show the changes in the study area in an anthropogenically influenced area. Based on the photos, the changes can be divided into the following categories:

1. debris pile - erosion
2. debris pile - accumulation
3. movable object
4. vegetation.

It is conceivable that CD can be identified not only by comparison between data sets of the same mission. By determining the distance between survey 1 of mission i and survey 2 of another mission, differences in the multitemporal images can also potentially be identified. As an example, the difference between M1 survey 1 and M17 survey 2 is shown in Fig. 9.

## Discussion

### Determination of suitable recording parameters for photogrammetric surveying in the Laufer Muehle area

After the exclusion of missions based on.

- long flight durations,
- high number of images,
- or high RMS values.

Only missions M5, M16 and M17 remained, which showed acceptable accuracy values and could potentially be used within the framework of the planned investigations.

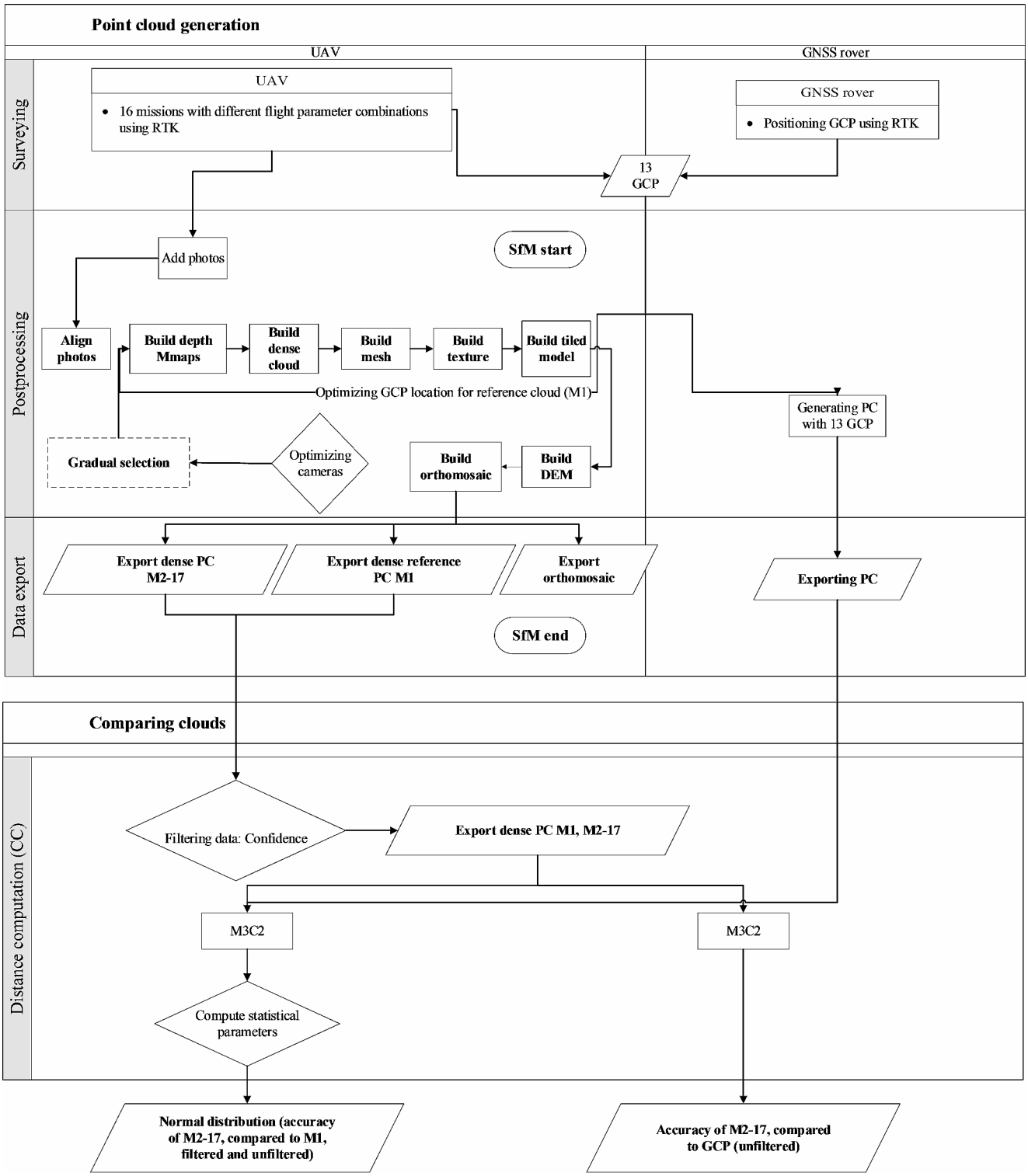


**Fig. 4** Processing sequence in distance determination between reference datasets (M1 and GCP) and the results of the different parameter combinations to determine the accuracy of datasets from missions with different acquisition parameters

**Table 4** Number of points of the PC from the SfM process, unfiltered and filtered (using confidence value), as well as an indication of the percentage filtered and the point differences between surveys 1 and 2

| | survey 1 | | | survey 2 | | | | |
|---|---|---|---|---|---|---|---|---|
| Mission | Points unfiltered [$10^6$] | Points filtered (confidence) [$10^6$] | Filtered [%] | Points unfiltered [$10^6$] | Points filtered (confidence) [$10^6$] | Filtered [%] | ΔPoints: survey1-survey2_unfiltered [%] | ΔPoints: survey1-survey2_filtered [%] |
| M1 | 349.1 | 273.0 | 21.8 | 290.8 | 245.6 | 15.5 | 16.7 | 10.0 |
| M5 | 112.2 | 94.3 | 16.0 | 102.4 | 87.5 | 14.5 | 8.8 | 7.2 |
| M16 | 54.5 | 46.0 | 15.5 | 53.1 | 43.9 | 17.2 | 2.6 | 4.6 |
| M17 | 79.8 | 64.5 | 19.1 | 75.3 | 60.7 | 19.4 | 5.7 | 6.0 |

**Table 5** Optimized parameters (case 21) developed from the sensitivity analysis for the M3C2 distance comparison in the study area and the resulting calculation results

| | |
|---|---|
| **projection scale [m]** | **0.8783** |
| **max depth [m]** | **2.5** |
| Gauss mean [m] | -0.182 |
| std. dev. [m] | 0.194 |
| RMS [m] | 0.265 |

M5 and M16 were conducted with comparable parameters but differed in terms of flight altitude and vertical overlap.

Although M5 was conducted with parameters that typically should lead to better accuracy results (lower flight altitude, higher vertical overlap and consequently a higher number of images), the RMS value, as presented in Fig. 5, showed only a slight deviation from the values of M16 in both the GCP and M1 comparisons. Thus, the increase in flight altitude from 80 to 110 m had no significant negative impact on the accuracy of the calculation results.

Missions M16 and M17 differed solely in terms of flight mode, leading to differences in flight duration and the number of images. In the context of high frequency acquisition, missions M5 and M17 are associated with a longer flight duration than M16 and. In case of M5, there is a relatively high resulting number of images, leading to an extended processing time during post-processing.

M16 generally showed better results compared to M5. Since significant differences in RMS values emerged between M16 and M17 (RMS values for M17 noticeably lower than those for M16), mission M17 was chosen as the preferred variant for flood investigations in the Laufer Muehle area.

As it was not possible to investigate the possibilities for the detection of water surfaces during a FE within the scope of these investigations, it cannot be excluded that good results (in a shorter time) can be achieved with the parameters of M16.

The total duration required for processing the photo images as part of the processing sequence shown in Fig. 4 could not yet be fully determined as part of these investigations. After this duration can be determined, an assessment of the recording capabilities of the M16 and M17 missions is possible and a final statement can be made on the selection of suitable survey parameters for data acquisition during a flood event. Accordingly, further investigations need to be conducted, considering the recording parameters of M16 and M17.

Due to the higher accuracies, M17 is better suited for the identification of CD. Therefore, the results from M17 were focused on for the identification of CD in the further course of this research.

## Analysis of CD results

Figures 7 and 8 show that regarding vegetation, areas were identified where significant changes occurred between the two surveys. However, it was also noted that although data were filtered (by confidence value and by M3C2 distance), vegetation was still present as noise. Especially in the context of automated detection and categorization, which is an aim of this and further investigations, it is still necessary to develop further methods for filtering noise in this respect or to optimize the existing methods.

A comparison of Figs. 7 and 8 shows that both localization and extent of change were present to a very similar degree, and change could be similarly divided into different categories in both images. However, the PC with photorealistic coloring also shows a different level of detail in the surface structure, with M1 showing a better mapping of the surrounding area than M17.

In Fig. 6, changes in the study area are particularly apparent in areas with vegetation cover. In principle, the representation of changes in these areas is desirable, but since they are for the most part scattering points (noise), these points hardly indicate risk areas in the case of a FE. This again shows that further improvement of the methods is necessary to be able to achieve a suitable separation of CD due to noise and CD due to significant changes in the terrain.

Further changes can be seen at the edges of the PC. These areas are usually where the largest inaccuracies occur in SfM processes, so the changes identified there are negligible.

a)

| mission | flight mode | flight altitude [m] | GSD [cm/Pixel] | flight velocity [m/s] | camera tilt [°] | horizontal overlap [%] | vertical overlap [%] | shutter priority [s] | flight duration [min] | number of images [-] |
|---|---|---|---|---|---|---|---|---|---|---|
| M1 | DG | 50 | 1.37 | 3 | 60 | 60 | 80 | no | 51:45 | 950 |
| M5 | NG | 80 | 2.19 | 4 | 60 | 60 | 80 | no | 14:00 | 214 |
| M16 | NG | 110 | 3.01 | 4 | 60 | 60 | 60 | no | 10:04 | 59 |
| M17 | DG | 110 | 3.01 | 4 | 60 | 60 | 60 | no | 15:24 | 90 |

b)

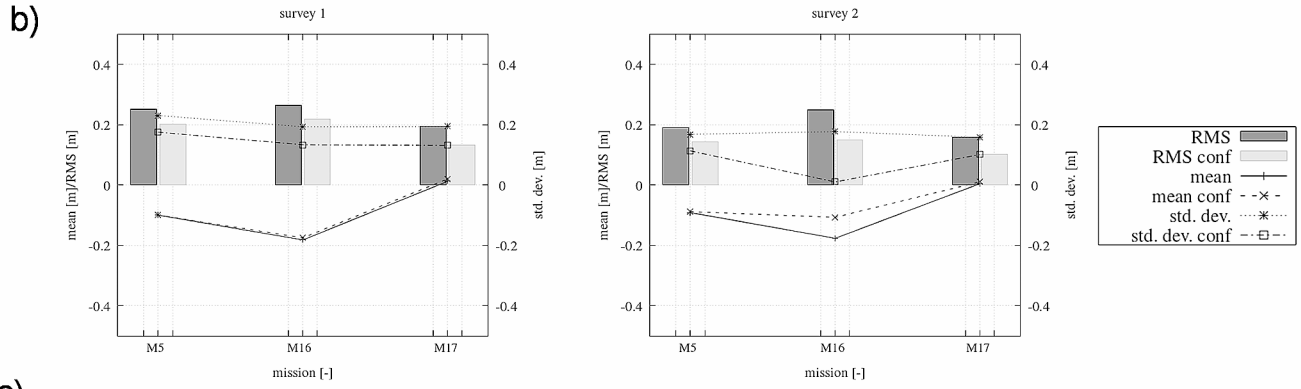


c)

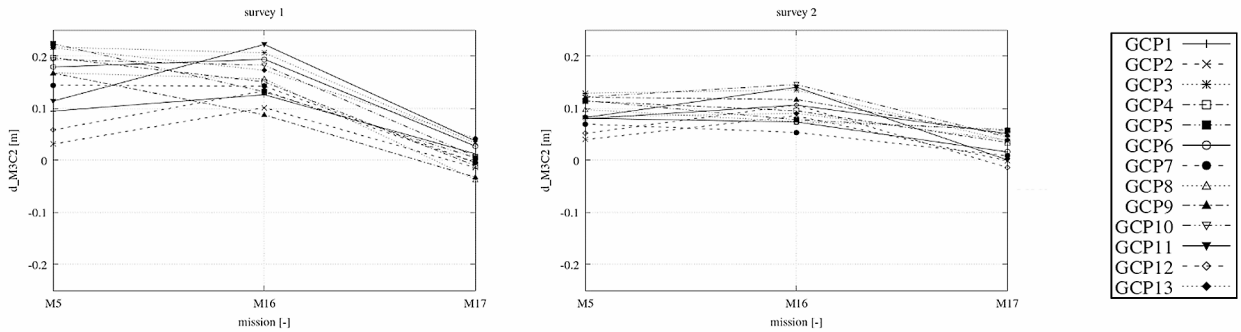


d)

| mission | ΔGCP - survey 1 $d_{mean}$GCP - survey 1 [m] | ΔGCP - survey 1 $d_{mean}$GCP - survey 2 [m] | ΔM1 - survey 1 unfiltered mean [m] | ΔM1 - survey 1 unfiltered std. dev. [m] | ΔM1 - survey 1 unfiltered RMS [m] | ΔM1 - survey 1 filtered mean [m] | ΔM1 - survey 1 filtered std. dev. [m] | ΔM1 - survey 1 filtered RMS [m] | ΔM1 - survey 2 unfiltered mean [m] | ΔM1 - survey 2 unfiltered std. dev. [m] | ΔM1 - survey 2 unfiltered RMS [m] | ΔM1 - survey 2 filtered mean [m] | ΔM1 - survey 2 filtered std. dev. [m] | ΔM1 - survey 2 filtered RMS [m] |
|---|---|---|---|---|---|---|---|---|---|---|---|---|---|---|
| M1 | - | - | - | - | - | - | - | - | - | - | - | - | - | - |
| M5 | 0.154 | 0.091 | -0.1 | 0.231 | 0.251 | -0.099 | 0.175 | 0.201 | -0.091 | 0.168 | 0.191 | -0.088 | 0.113 | 0.143 |
| M16 | 0.155 | 0.1 | -0.182 | 0.193 | 0.265 | -0.175 | 0.134 | 0.22 | -0.176 | 0.177 | 0.25 | -0.107 | 0.106 | 0.151 |
| M17 | 0.021 | 0.032 | 0.013 | 0.194 | 0.195 | 0.021 | 0.131 | 0.133 | 0.005 | 0.158 | 0.158 | 0.011 | 0.101 | 0.102 |

**Fig. 5** **a** Flight parameters of M1, M5, M16-M17 with the indication of the flight durations as well as the number of images **b** mean value, standard deviation (std. dev.) and root mean square (RMS) resulting from M3C2 distance computation between M5, M16-M17 and the reference data set M1, **c** mean value, std. dev. and RMS of the vertical distances between the GCP and the dense PC from M5, M16-M17, **d** values used in **b** and **c**

The comparison of the identified changes shown in Fig. 9 (M1 survey 1 - M17 survey 2) with the images in Figs. 7 and 8 shows that the localities of the changes are comparable. However, the identified changes in Fig. 9 are shown to a lesser extent. Also, some changes, such as mass redistribution in the debris pile area, were not detected.

In principle, the comparison between surveys from different missions may lead to good results in CD. Since good


**Fig. 6** Areas with detected changes between survey 1 and 2 of M1 and M17 in the Laufer Muehle area ($|d_{M3C2}| \geqslant 0.25\ m$; red: elevation increase in survey 2; blue: elevation decrease in survey 2)

**Fig. 7** PC (M1) from surveys 1 and 2 with color coding of CD ($|d_{M3C2}| \geqslant 0.25\ m$; red: height increase in survey 2; blue: height decrease in survey 2)

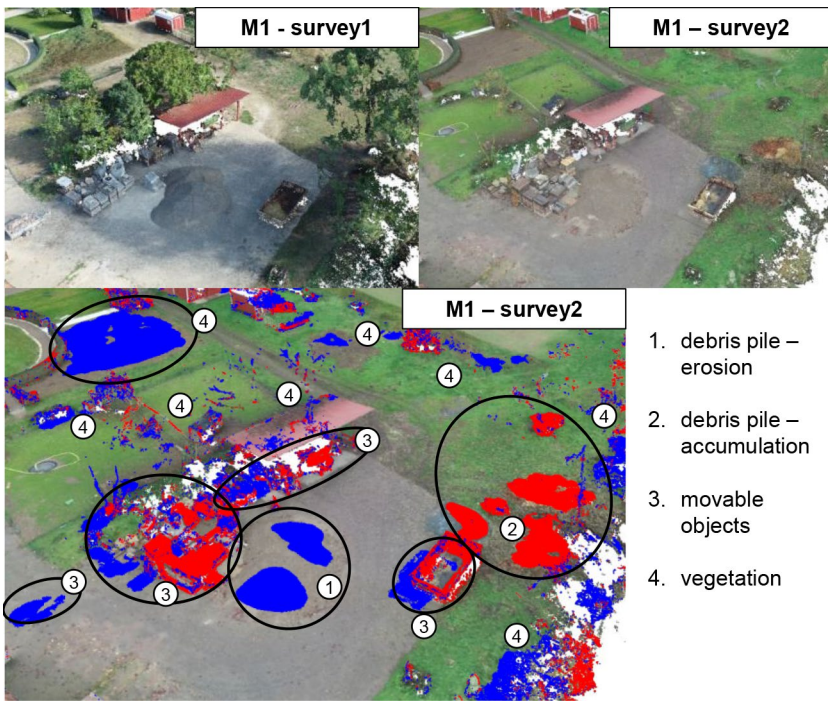

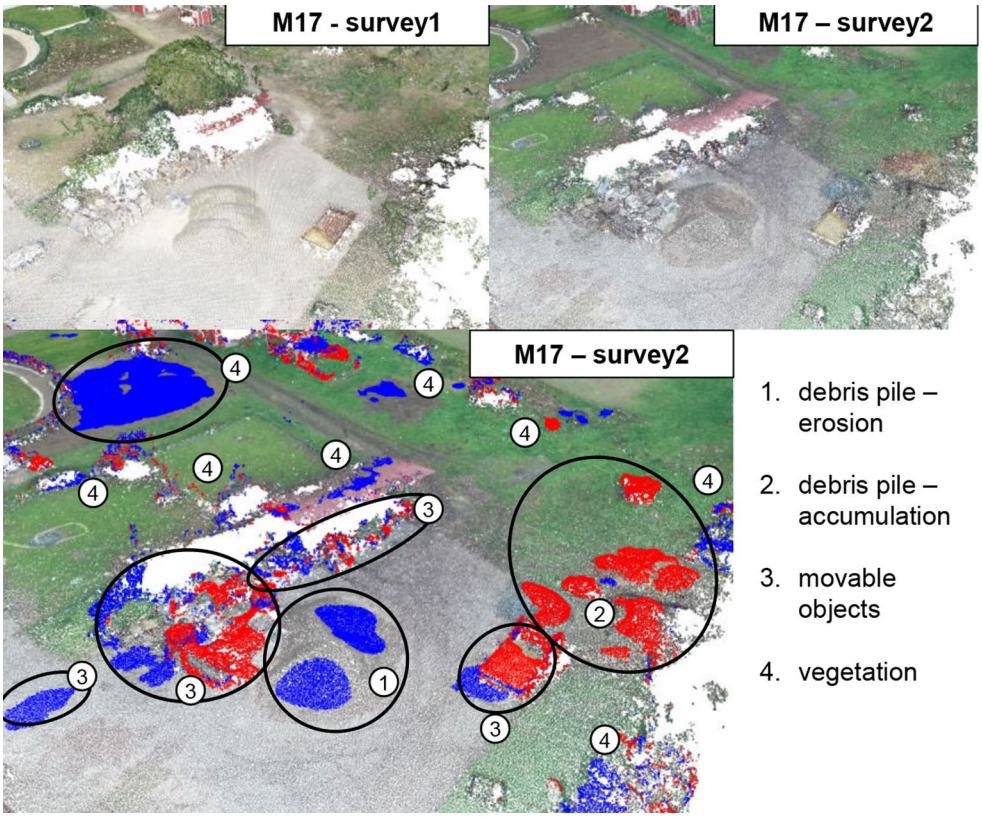


**Fig. 8** PC (M17) from surveys 1 and 2 with color coding of CD ($|d_{M3C2}| \geqslant 0.25\ m$; red: height increase in survey 2; blue: height decrease in survey 2)

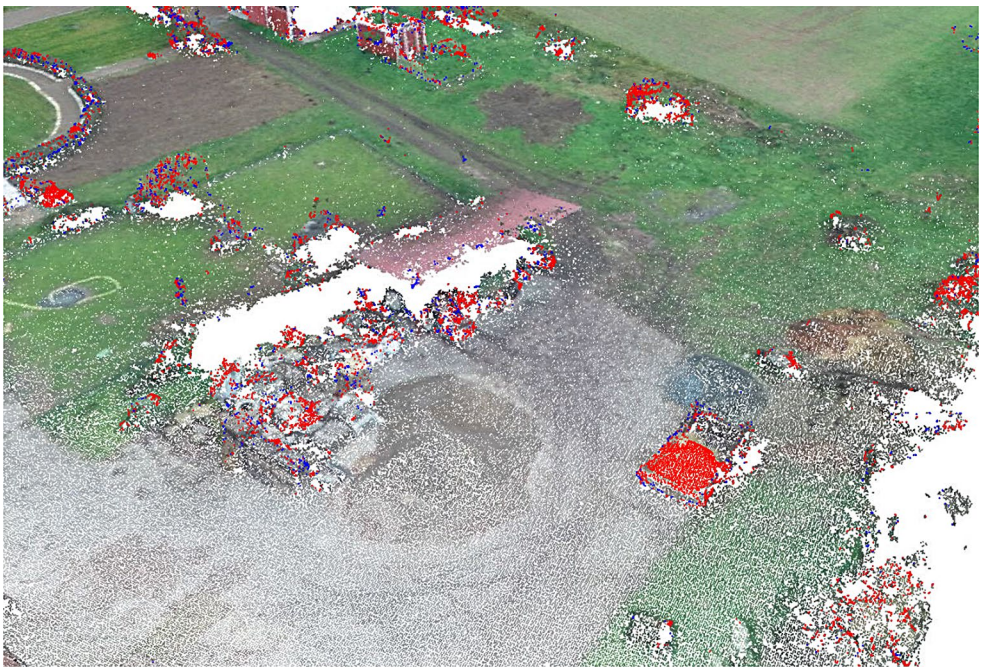

**Fig. 9** CD between M1 survey 1 and M17 survey 2 ($|d_{M3C2}| \geqslant 0.25\ m$; red: height increase in survey 2; blue: height decrease in survey 2)

results were obtained in the analysis of CD at M17 and these also agreed with the high-resolution data set M1, no further investigations were carried out in this context.

## Summary

For the photogrammetric analysis of flood events at the Aisch river using airborne imagery, investigations were carried out in the area of the Laufer Muehle. The area was to be imaged autonomously by an unmanned aerial vehicle (UAV) to determine and use an efficient flight parameter constellation (short flight duration with a low resulting number of images while maintaining sufficient accuracy within the results from Structure from Motion method (SfM)). This constellation should make it possible to image the study area at high frequency to detect changes in the terrain by multitemporal imaging (flood prevention) as well as to image the floodplains during a flood event (FE).

A total of 16 different flight parameter constellations (M2-M17) were investigated, with only a few variations yielding satisfying results (M1, M5, M16 and M17), which were then discussed accordingly. For accuracy analysis as well as to create an optimized reference dataset, 13 GCP were located in the study area and georeferenced using a GPS rover with RTK connectivity. The photos were acquired using a Phantom 4 RTK unit. 3D-data sets were generated by photogrammetric reconstruction using SfM. The data with the presumably most accurate parameter constellation (M2) was optimized by including the georeferenced GCP in the SfM process. This optimization resulted in the M1 reference dataset. An M3C2 distance computation was performed between the results of the SfM process and the georeferenced GCP, as well as the reference data set M1. Based on the analysis of normal distributions as well as different accuracy parameters (mean deviation, root mean square (RMS), standard deviation (std. dev.)), the results were evaluated based on their different recording parameters. Considering the accuracy values as well as the acquisition time and the number of images, variant M17 could be identified as suitable for CD acquisition before a FE, both in terms of time efficiency and accuracy aspects. Recording floodplains during a FE could not be investigated during this research due to a lack of data.

Significant changes ($|d_{M3C2}| \geqslant 0.25\ m$) in the study area could be detected by the M3C2 distance calculation between the M1 survey 1 and M1 survey 2 (highest accuracy of the data) as well as between the M17 survey 1 and M17 survey 2 (most effective), using calculation parameters determined in a sensitivity analysis. The categorization of the changes could be done manually in a focus area of the study area due to the photorealistic coloring of the measurement points.

## Future prospects

The edge areas in the photogrammetric data sets of an investigation area are usually mapped much less accurately than the center area, since this area is covered by a large number of overlapping photos, while there are only a few photos available of the edge areas. If the distance calculations discussed in Sect. M3C2: accuracy analysis of mission data by comparison with data set M1 were applied to a corresponding focal area without considering the edge areas, an improvement of the accuracy results discussed in Sect. 6.3 would be likely, especially in connection with the RMS and std. dev. values. Since this circumstance relates to all distance calculations performed, the evaluations of the individual missions performed in Sect. Discussion remain valid.

To integrate the CD process into flood prevention, the data must be correlated with existing flood models. For this purpose, suitable interfaces have to be created, which allow a quick analysis in the study area in case of flood hazard. For this purpose, the identified changes have to be analyzed and categorized in more detail. In this way, it is possible to identify movable material that moves as float material in a flood event and can lead to damage or blockage of structures. In this context, the PC that are being compared need to be better cleaned of noise in order to optimize the M3C2 process. There is significant potential in categorizing and summarizing various changes into individual components, leading to a better understanding of the structure of these changes. This approach should be implemented in future considerations.

These investigations were performed using relatively high SfM accuracy parameters, which may result in a correspondingly long processing time. The results obtained so far suggest that, in the context of plausible CD identification, these values should be considered a minimum. However, in the context of high-frequency recording of floodplains, it is conceivable that the analysis does not necessarily need to be performed using a PC, but that orthophotos can be used to estimate the two-dimensional location of floodplains. Since the accuracy studies conducted always referred to a 3D comparison, it cannot be excluded that the two-dimensional comparison (not considering the elevation component of the comparison vector) could lead to a good result for 2D localization. In this way, a significantly lower processing effort could be required within the SfM process. However, the possibilities in this context need to be determined in the context of a FE or tested on existing data from other investigations.

No additional camera calibration was performed prior to data acquisition. Only for the reference state M1, precalibration was refined based on the GCPs. To improve the accuracy of the measurement system used, future

investigations should include a comprehensive calibration. This approach may potentially allow for a better representation of small-scale changes in the study area, which were difficult to distinguish from noise in the described process and were consequently filtered out.

The flight parameter requirements determined within the scope of these investigations refer to the use of a Phantom 4 RTK UAV at a maximum flight altitude of 110 m and to the observation of an (in the case of a FE) relatively small observation area. Since FE usually have an impact on areas in the order of many square kilometers, it is necessary to investigate the scalability of the investigation results and possibly extend them to additional or different recording systems. A suitable approach is to compare the GSD, which is a measure of the resolution at which a survey area is mapped. With linear increases in flight altitude and camera resolution, the preservation of the accuracy statements made in this study is likely.

A disadvantage of the UAV measurement technique used in this research is that it cannot be used, or can only be used to a limited extent, during bad weather conditions (high wind speed, rain). Since these weather conditions usually accompany an FE, the approach proposed here is not fully applicable during an FE. Thus, it is necessary to extend the results of these investigations to the use of alternative aerial vehicle which can be operated during bad weather conditions.

The high-frequency representation of floodplains using orthophotos can lead to a good estimation of the development of the floodplain. To be able to determine a corresponding increase or decrease of the area, as well as the water depth resulting from the flooding, it is necessary to extract the water area from these data. Extensive research already exists for this purpose, which is often based on the use of AI-supported (artificial intelligence) technologies. Different deep learning methods for floodplain imaging are discussed, for example, in Bentivoglio et al. (2021), Gebrehiwot and Hashemi-Beni (2020), Hernández et al. (2022). The implementation of such systems is usually associated with a high effort and requires an extensive data basis for teaching the algorithm, which is why the feasibility of these methods for the Laufer Muehle study has to be determined in the course of further investigations.

**Supplementary Information** The online version contains supplementary material available at https://doi.org/10.1007/s12518-024-00561-y.

**Author's contributions** M.K. contributed to the study conception and design, material preparation and data collection, data analysis, and creation of the manuscript. D.C. contributed to the study conception and design, data evaluation and reviewing the draft. All authors approved this version to be published.

**Funding** The research was supported by the STAEDTLER foundation. The financial support included coverage of costs for travel, material/equipment, and personnel costs.
Open Access funding enabled and organized by Projekt DEAL.

**Data availability** The datasets generated during and/or analyzed during the current study are available from the corresponding author upon reasonable request.

**Code availability** Not applicable.

## Declarations

**Conflicts of interest** Not applicable.



## References

Agisoft LLC (2022a) Agisoft Metashape User Manual: Professional Edition, Version 1.8

Agisoft LLC (2022b) Metashape Python Reference: Release 1.8.4

Baltsavias EP (1999a) A comparison between photogrammetry and laser scanning. ISPRS J Photogrammetry Remote Sens 54:83–94. https://doi.org/10.1016/S0924-2716(99)00014-3

Bayerische S (2010) Anlage 1 BayWG - Verzeichnis der Gewässer erster Ordnung. https://www.gesetze-bayern.de/Content/Document/BayWG-ANL_1. Accessed 26 August 2022

Bayerisches Landesamt für Umwelt (2022b) Gewässerkundlicher Dienst Bayern: Stammdaten Laufermühle. https://www.gkd.bayern.de/de/fluesse/wasserstand/bayern/laufermuehle-24263000. Accessed 24 August 2022

Bayerisches Landesamt für Umwelt (2022a) Angewandte Geologie: Ursprung der Aisch WSW von Illesheim. https://www.umweltatlas.bayern.de/mapapps/resources/reports/sb_geotope/generateBericht.pdf?additionallayerfieldvalue=575Q003

Bayerisches Landesamt für Umwelt (2016) Verzeichnis der Bach- und Flussgebiete in Bayern: Flussgebiet Main. https://www.lfu.bayern.de/wasser/gewaesserverzeichnisse/doc/tab24.pdf#page=70. Accessed 25 August 2022

Bayerisches Landesamt für Umwelt (2011) Entwurf Einer Kulturlandschaftlichen Gliederung Bayerns als Beitrag Zur Biodiversität. 17:Aischgrund

Hochwassernachrichtendienst Bayern: Stammdaten Laufermühle / Bayerisches Landesamt für Umwelt, Aisch (2023) https://www.hnd.bayern.de/pegel/regnitz/laufermuehle-24263000/stammdaten? Accessed 2 January 2023

Bentivoglio R, Isufi E, Jonkman SN, Taormina R (2021) Deep learning methods for Flood Mapping. A Review of Existing Applications and Future Research Directions

Cawood AJ, Bond CE, Howell JA, Butler RWH, Totake Y (2017) LiDAR, UAV or compass-clinometer? Accuracy, coverage and the effects on structural models. J Struct Geol 98:67–82. https://doi.org/10.1016/j.jsg.2017.04.004

de Waele J, Fabbri S, Santagata T, Chiarini V, Columbu A, Pisani L (2018) Geomorphological and speleogenetical observations using terrestrial laser scanning and 3D photogrammetry in a gypsum cave (Emilia Romagna, N. Italy). Geomorphology 319:47–61. https://doi.org/10.1016/j.geomorph.2018.07.012

Dinkel A, Hoegner L, Emmert A, Raffl L, Stilla U (2020) Change detection in photogrammetric point clouds for monitoring of alpine, gravitational mass movements. ISPRS Ann. Photogramm. Remote Sens Spat Inf Sci V –2–2020:687–693. https://doi.org/10.5194/isprs-annals-V-2-2020-687-2020

El-Din Fawzy H (2019) 3D laser scanning and close-range photogrammetry for buildings documentation: a hybrid technique towards a better accuracy. Alexandria Eng J 58:1191–1204. https://doi.org/10.1016/j.aej.2019.10.003

Eltner A, Hoffmeister D, Kaiser A, Karrasch P, Klingbeil L, Stöcker C, Rovere A (eds) (2022) UAVs for the environmental sciences: methods and applications. wbg Academic, Darmstadt

Fischler MA, Bolles RC (1981) Random sample consensus. Commun ACM 24:381–395. https://doi.org/10.1145/358669.358692

Forlani G, Dall'Asta E, Diotri F, Di Cella UM, Roncella R, Santise M (2018) Quality Assessment of DSMs produced from UAV flights georeferenced with On-Board RTK positioning. Remote Sens 10:311. https://doi.org/10.3390/rs10020311

Gebrehiwot A, Hashemi-Beni L (2020) A Method to Generate Flood Maps in 3d Using dem and Deep Learning. Int. Arch. Photogramm. Remote Sens. Spatial Inf. Sci. XLIV-M-2-2020:25–28. https://doi.org/10.5194/isprs-archives-XLIV-M-2-2020-25-2020

Grussenmeyer P, Landes T, Voegtle T, Ringle K (2008) Comparison methods of terrestrial laser scanning, photogrammetry and tacheometry data for recording of cultural heritage buildings. The International Archives of the Photogrammetry, Remote Sensing and Spatial Information Sciences. Vol. XXXVII. Part B5. Beijing 2008

Hernández D, Cecilia JM, Cano J-C, Calafate CT (2022) Flood Detection using Real-Time Image Segmentation from Unmanned Aerial vehicles on Edge-Computing platform. Remote Sens 14:223. https://doi.org/10.3390/rs14010223

James MR, Robson S, Smith MW (2017) 3-D uncertainty-based topographic change detection with structure-from-motion photogrammetry: precision maps for ground control and directly georeferenced surveys. Earth Surf Process Land 42:1769–1788. https://doi.org/10.1002/esp.4125

Kögel M, Pflitsch A, Northup DE, Carstensen D, Medley JJ, Mansheim T, Killing T, Buschbacher M, Angerer H, Falkner J, Kynatidis A, Ott V, Regler S (2022) Combination of close-range and aerial photogrammetry with terrestrial laser scanning to answer microbiological and climatological questions in connection with lava caves. Appl Geomat. https://doi.org/10.1007/s12518-022-00459-7

Kutschera G, Blankenbach J, Blut C, Bolle F-W, Effkemann C, Gahlaut S, Hein N, Jagow M-L, Schüttrumpf H, Schwermann R, Tabatabaei S, Wöffler T (2018) Monitoring kleiner und mittlerer Fließgewässer mittels bemannter und unbemannter Wasserfahrzeuge – Ergebnisse Des Projektes RiverView. Hydrol Und Wasserbewirtsch / BfG – Jahrgang: 62 2018 6. https://doi.org/10.5675/HyWa_2018.6_5. ISSN 1439–1783

Lague D, Brodu N, Leroux J (2013) Accurate 3D comparison of complex topography with terrestrial laser scanner: application to the Rangitikei canyon (N-Z). ISPRS J Photogrammetry Remote Sens 82:10–26. https://doi.org/10.1016/j.isprsjprs.2013.04.009

Luhmann T (2013) Combination of Photogrammetry and Terrestrial Laserscanning – potentials and limitations, Part 2: systems, algorithms and Applications. Adv Geodetic Sci Ind :81–90

Luhmann T (2018) Nahbereichsphotogrammetrie: Grundlagen - Methoden -Beispiele, 4th edn. Wichmann, Berlin, Offenbach

Mancini F, Salvini R (2020) Applications of Photogrammetry for Environmental Research. MDPI - Multidisciplinary Digital Publishing Institute

Marín-Buzón C, Pérez-Romero AM, León-Bonillo MJ, Martínez-Álvarez R, Mejías-García JC, Manzano-Agugliaro F (2021) Photogrammetry (SfM) vs. terrestrial laser scanning (TLS) for Archaeological excavations: Mosaic of Cantillana (Spain) as a case study. Appl Sci 11:11994. https://doi.org/10.3390/app112411994

Meydenbauer A (1867) Die Photometrographie: Wochenblatt Des Architektenvereins zu Berlin Jg. 1, 1867, Nr. 14, S. 125–126; Nr. 15, S. 139–140; Nr. 16, S. 149–150

Mora-Felix ZD, Sanhouse-Garcia AJ, Bustos-Terrones YA, Loaiza JG, Monjardin-Armenta SA, Rangel-Peraza JG (2020) Effect of photogrammetric RPAS flight parameters on plani-altimetric accuracy of DTM. Open Geosci 12:1017–1035. https://doi.org/10.1515/geo-2020-0189

Mulsow C, Mandlburger G, Ressl C, Maas H-G (2019) Vergleich von Bathymetriedaten aus luftgestützter Laserscanner- und Kameraerfassung. Dreiländertagung der DGPF, der OVG und der SGPF in Wien, Österreich. Publikationen der DGPF

Nota EW, Nijland W, de Haas T (2022) Improving UAV-SfM time-series accuracy by co-alignment and contributions of ground control or RTK positioning. Int J Appl Earth Obs Geoinf 109:102772

Przybilla H-J, Bäumker M (2020) Untersuchungen zur Qualität Des Realtime Kinematic GNSS systems Der DJI Phantom 4 RTK. 40 Wissenschaftlich-Technische Jahrestagung Der DGPF Stuttgart Publikationen der DGPF:47–61

Qin R, Tian J, Reinartz P (2016) 3D change detection – approaches and applications. ISPRS J Photogrammetry Remote Sens 122:41–56. https://doi.org/10.1016/j.isprsjprs.2016.09.013

Rusinkiewicz S, Levoy M (2001) Efficient variants of the ICP algorithm. In: Proceedings / Third International Conference on 3-D Digital Imaging and Modeling: 28 May – 1 June 2001, Quebec City, Canada. IEEE Computer Soc, LosAlamitos, Calif., pp 145–152

SAPOS (2015) Produktdefinition SAPOS. https://www.sapos.de/files/SAPOS-Produktdefinition_2017.pdf

Talha A, Fritsch D (2019) Integration of laser scanning and photogrammetry in 3D4D Cultural Heritage: a review. IJAST 9:76–91

Triantafyllou A, Watlet A, Le Mouélic S, Camelbeeck T, Civet F, Kaufmann O, Quinif Y, Vandycke S (2019) 3-D digital outcrop model for analysis of brittle deformation and lithological mapping (Lorette cave, Belgium). J Struct Geol 120:55–66. https://doi.org/10.1016/j.jsg.2019.01.001

Vosselman G, Maas H-G (eds) (2011) Airborne and terrestrial laser scanning. Whittles; CRC, Dunbeath, Boca Raton, Fla

Wasserwirtschaftsamt Nürnberg (2021) Luftbilder HW2021

Wiggenhagen M, Steensen T (2021) Taschenbuch Zur Photogrammetrie Und Fernerkundung: = guide for photogrammetry and remote sensing, 6th edn. Wichmann, Berlin, Offenbach

Winiwarter L, Anders K, Höfle B (2021) M3C2-EP: pushing the limits of 3D topographic point cloud change detection by error propagation. ISPRS J Photogrammetry Remote Sens 178:240–258. https://doi.org/10.1016/j.isprsjprs.2021.06.011

Xie H, Wang H, Yang Y, Chen Y, Yang J, Wang S, Liu Z (2021) Analysis of Underwater Topographic Survey of Stilling Basin based on unmanned Survey System. Adv Mater Sci Eng 2021:1–15. https://doi.org/10.1155/2021/5514165